INL/CON-16-37753
PREPRINT

Gap Size Uncertainty Quantification in Advanced Gas Reactor TRISO Fuel Irradiation Experiments

11th International Topical Meeting on Nuclear Reactor Thermal-Hydraulics, Operations and Safety (NUTHOS-11) (2016)

Binh T. Pham, Jeffrey J. Einerson,
Grant L. Hawkes, Nancy J. Lybeck,
David A. Petti

October 2016

The INL is a
U.S. Department of Energy
National Laboratory
operated by
Battelle Energy Alliance

Gap Size Uncertainty Quantification in Advanced Gas Reactor TRISO Fuel Irradiation Experiments

Binh T. Pham*, Jeffrey J. Einerson, Grant L. Hawkes, Nancy J. Lybeck, and David A. Petti
Idaho National Laboratory
P.O. Box 1625, Idaho Falls, Idaho, 83415, United States of America
Binh.Pham@inl.gov, Jeffrey.Einerson@inl.gov, grant.hawkes@inl.gov, Nancy.Lybeck@inl.gov, David.Petti@inl.gov

ABSTRACT

The Advanced Gas Reactor (AGR)-3/4 experiment is the combination of the third and fourth tests conducted within the tristructural isotropic fuel development and qualification research program. The AGR-3/4 test consists of twelve independent capsules containing a fuel stack in the center surrounded by three graphite cylinders and shrouded by a stainless steel shell. This capsule design enables temperature control of both the fuel and the graphite rings by varying the neon/helium gas mixture flowing through the four resulting gaps. Knowledge of fuel and graphite temperatures is crucial for establishing the functional relationship between fission product release and irradiation thermal conditions. These temperatures are predicted for each capsule using the commercial finite-element heat transfer code ABAQUS. Uncertainty quantification reveals that the gap size uncertainties are among the dominant factors contributing to predicted temperature uncertainty due to high input sensitivity and large uncertainty. Gap size uncertainty originates from the fact that all gap sizes vary with time due to dimensional changes of the fuel compacts and three graphite rings caused by extended exposure to high temperatures and fast neutron irradiation. Gap sizes are estimated using as-fabricated dimensional measurements at the start of irradiation and post irradiation examination dimensional measurements at the end of irradiation. Uncertainties in these measurements provide a basis for quantifying gap size uncertainty. However, lack of gap size measurements during irradiation and lack of knowledge about the dimension change rates lead to gap size modeling assumptions, which could increase gap size uncertainty. In addition, the dimensional measurements are performed at room temperature, and must be corrected to account for thermal expansion of the materials at high irradiation temperatures. Thus uncertainty in the thermal expansion coefficients for the graphite materials used in the AGR-3/4 capsules also increases gap size uncertainty. This study focuses on analysis of modeling assumptions and uncertainty sources to evaluate their impacts on the gap size uncertainty and, subsequently, on uncertainty of calculated temperatures.

KEYWORDS

Thermal model, Uncertainty quantification, Fuel irradiation, Graphite dimension change.

1. INTRODUCTION

The Advanced Gas Reactor (AGR)-3/4 experiment is the combination of the third and fourth tests conducted within the tristructural isotropic (TRISO) fuel development and qualification research program. The main objectives of the TRISO fuel irradiation are to provide the necessary data on fuel performance to support qualification of fuel design and fabrication process for normal operation and postulated accident conditions, and support development and validation of fuel performance and fission product transport models and codes [1]. The AGR 3/4 experiment was inserted in the northeast flux trap position in the Advanced Test Reactor (ATR) core at Idaho National Laboratory in December

2011 and successfully completed in April 2014, resulting in irradiation of the TRISO fuel for 369 effective full power days (EFPDs).

The AGR-3/4 test consists of twelve independent capsules containing TRISO uranium oxy-carbide fuel particles embedded in four cylindrical compacts stacked on top of each other. Every fuel compact contains designed-to-fail fuel particles that will provide a known source of fission products for subsequent transport through the compact matrix and structural graphite materials. It is essential that irradiated fuel temperature is maintained within a specified temperature range similar to the desired thermal condition of the high temperature gas-cooled reactor. The contact between thermocouple (TC) and test fuel particles embedded in compacts could lead to unwanted particle failure; therefore the fuel temperature could not be measured. Instead, each capsule is instrumented with two or three TCs embedded in the graphite rings enabling temperature control. The predefined target TC temperature is used as a feedback for the gas flow controller to delivered necessary neon/helium gas mixture to maintain desired fuel temperature.

The thermal analysis has been performed separately on each capsule for each day during the entire irradiation campaign. The commercial finite-element heat transfer code ABAQUS was used for this thermal analysis to predict fuel temperatures for all capsules as discussed in [2,3,4]. The thermal model involves complex physical mechanisms (e.g., fuel compact and graphite material shrinkage) and properties (e.g., fuel compact conductivity and density), which are not fully and accurately quantified due to lack of relevant data. Therefore, the thermal model predictions are affected by uncertainty in input parameters and by incomplete knowledge of the underlying physics leading to modeling assumptions. Along with the deterministic predictions from a set of input thermal conditions, information about prediction uncertainty is instrumental for the Advanced Reactor Technologies program decision-making. Well defined and reduced uncertainty in model predictions helps increase the quality of and confidence in the AGR technical findings [5].

Within the TRISO fuel irradiation campaign, the AGR-1 and AGR-2 experiments were completed before AGR-3/4. The input uncertainty quantification for AGR-1 and AGR-2 calculated temperatures was described in detail in [4]. The uncertainty analysis results reveal that the uncertainty of the gap size is among the most influential factors contributing to calculated temperature uncertainty. Typically, under neutron irradiation, graphite materials shrink or swell leading to changes in gap sizes. As a result, the variable gap size models are used in thermal models for AGR-1, AGR-2, and AGR-3/4 capsules as described in [2,3,4].

The gap size uncertainties originate from lack of direct experimental data for accurate estimation of dimensional change rates of fuel compacts and graphite rings. Previously, the gap size uncertainty is assumed to be increasing gradually from the gap size uncertainty at the start of irradiation (or as-fabricated gap size uncertainty) to 50% more at the end of irradiation [6]. However, the diameters of fuel compacts and the three graphite rings measured during the AGR-3/4 post irradiation examination (PIE) are used to calculate gap sizes at the end of irradiation, which could lead to the gap size uncertainty reduction in all capsules. This works focuses on the uncertainty quantification of the gap sizes based on uncertainties of the PIE measurements. Also, the diameters used for gap size calculations are measured at room temperature, and then these gap sizes are corrected accounting for the graphite thermal expansion at high temperature during irradiation. The impact of the uncertainty of graphite thermal expansion coefficient on the uncertainty of gap sizes is also considered.

2. THERMAL MODEL AND UNCERTAINTY ANALYSIS

2.1. Thermal Model Description

An AGR-3/4 capsule has a stack of four fuel compacts in the center surrounded by three graphitic annuli: proceeding from the compact out are the inner ring, outer ring, and sink ring as shown on the

left side of Fig. 1. This design leads to four temperature control gas gaps: Gap 1 between the fuel stack and inner surface of the inner ring, Gap 2 between the inner ring and inner surface of the outer ring, Gap 3 between the outer ring and inner surface of the sink ring, and Gap 4 between the sink ring and inner surface of capsule shell. Gap 1 and Gap 2 are small (< 0.1 mm) to maintain high temperature for the inner and outer rings. Gaps 3 and 4 are larger, allowing better control for fuel compact and graphite ring temperatures.

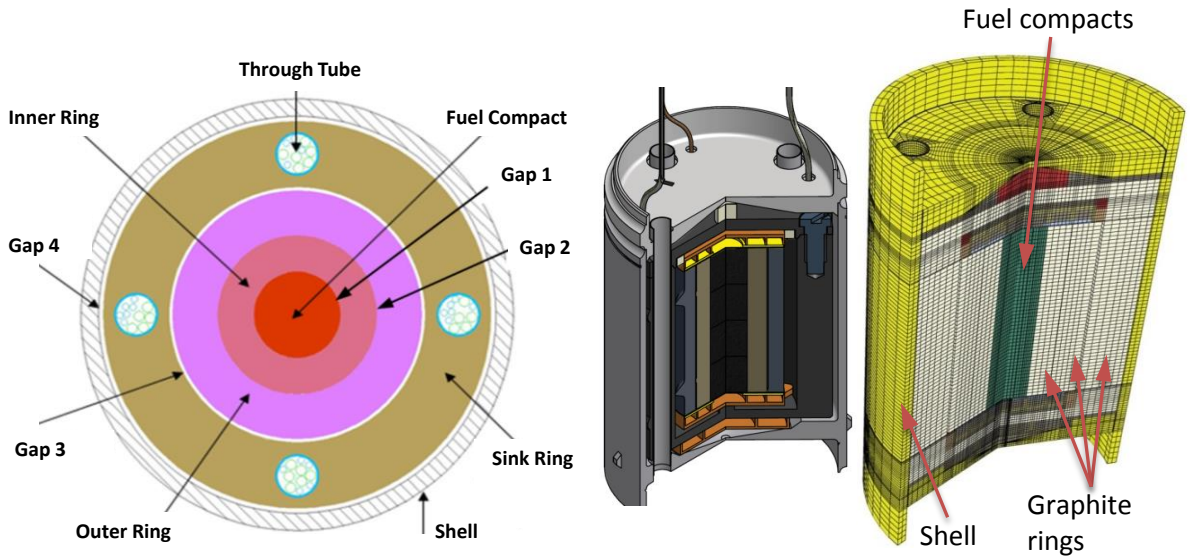

Fig. 1. AGR-3/4 capsule cross-sectioned view (left), Cutaway view (middle), and finite-element mesh (right) of an AGR-3/4 capsule.

The commercial finite-element heat transfer code ABAQUS was used to create a thermal model for each capsule to predict fuel and graphite temperatures for each day during the entire irradiation time. Fig. 1 shows the cutaway view in the middle and finite element mesh with colored entities on the right side for an AGR-3/4 capsule. A basic mesh was created for one capsule in each AGR experiment. This mesh was propagated to all other capsules by varying gas gap conductivity and gap conductance to compensate for individual capsule gap dimension and changes in the gap size during irradiation. The model details, including model validation and verification, calibration, sensitivity analysis, and results are described in [2].

Fission power generated in the fuel compacts and three graphite rings is mainly conducted and radiated out through the four gaps between surfaces of the fuel stack, the three graphite rings, and the stainless steel shell to the ATR primary cooling water, which serves as the ultimate heat sink for all capsules. The governing equations of steady-state conduction and radiation heat transfer are used for the thermal models. An adiabatic boundary condition was placed on the top and bottom of each capsule. A heat transfer coefficient connected to the cooling water was placed on the outside of the capsule shell. The cooling water temperature is matched within 0.5˚C of the calculated temperatures, which indicates good modeling performance. The thermal models were calibrated globally for all twelve capsules to reasonably match calculated and measured TC temperatures during the first irradiation cycle, when TC readings were deemed reliable. The surface emissivity of the three graphite rings and stainless steel shell and the graphite thermal expansion coefficient are adjusted within their uncertainty bounds similarly in all capsule thermal models.

2.2. Model Bias

Continued monitoring of TC residuals (measured minus calculated TC temperatures), as a function of EFPD beyond the calibration period, shows a pattern of non-zero averaged values in several capsules. This suggests the existence of model bias. The model biases, calculated as the ratio between the averaged TC residual and averaged TC temperature during the first three ATR cycles, are presented in Table 1 for twelve capsules. TC residuals for the later cycles are not used for estimating model bias to avoid the increased risk of using potentially inaccurate measurements due to possible TC drift failures under the extended high temperature and fast neutron irradiation. Capsules 5, 7, 9, and 10 have negligible model bias (<1%) due to small average of their TC residuals (<5°C), indicating excellent fit between measured and calculated TC temperatures in these capsules. Model biases for the remaining capsules are moderate, with the exception that Capsule 11 has the largest model bias of -9.9% based on the average of −74°C for its TC residuals.

Table 1. Thermal model biases for 12 AGR-3/4 capsules.

Capsule	1	2	3	4	5	6	7	8	9	10	11	12
Model Bias, %	3.6	1.4	2.0	1.4	0.5	1.9	0.6	2.4	0.1	-0.6	-9.9	-4.7

2.3. Model Input Uncertainty

The first step in temperature uncertainty quantification is to identify the model parameters of potential importance to the calculated temperatures. The identification is based on a thorough analysis of all uncertainty sources and modeling assumptions. The selected parameters either have high sensitivity to calculated temperatures and/or have large input uncertainty, resulting in large impacts on temperature uncertainty. The standard uncertainty propagation method is used to combine input uncertainties and sensitivities to quantify the overall uncertainty of calculated temperatures as described in [6].

Accurate estimation of input uncertainties is crucial for quantification of temperature uncertainty. Ideally, uncertainties of inputs are directly estimated from measurements uncertainties (e.g., neon fraction of the gas mixture and as-fabricated gap size). When input data are the results from other simulation codes, their uncertainties are estimated by the modelers, taking into account all uncertainty sources in their codes (e.g., uncertainties of fuel and graphite heat rates taken from the fuel depletion codes). Finally, expert judgment is used as the basis to specify the uncertainty range for those inputs taken from legacy experiments (e.g., fuel compact and graphite thermal conductivities). Notably, some input uncertainties are dynamic during the course of irradiation, accounting for the effects of unplanned events and changes in thermal properties of capsule components due to exposure to high temperature and fast neutron irradiation (e.g., neon fraction and gap sizes).

A sensitivity coefficient for an input parameter is the ratio of the change in predicted temperature to the associated change in input parameter. Thus, the input sensitivity measures how the calculated temperature would be influenced by changes in an input parameter. For the first-order sensitivity analysis, a series of cases was compared to a base case by varying each input to the thermal model [7]. The bar charts in Fig. 2 represent the variations of peak fuel temperature in the AGR-3/4 Capsule 5 at EFPD 80 (Time Step 30 of ATR Cycle 152B) when each input varies by ±10%. The temperature variations are sorted from largest to smallest, so the most sensitive inputs are located at the top of the charts. Thus, the top three sensitive parameters are heat rate in the fuel compacts, neon fraction of the gas mixture, and Gap 4 size. The next three are fuel thermal conductivity, Gap 1 size, and Gap 3 size. The ±10% variations of graphite heat rate, graphite thermal conductivity, and graphite emissivity caused notable variations in peak fuel temperature. It is worth mentioning that input sensitivities and their rankings change with time and the location of the predicted temperatures. However, fuel heat rate, neon fraction, and gap sizes essentially remain among the most sensitive parameters for all calculated temperatures.

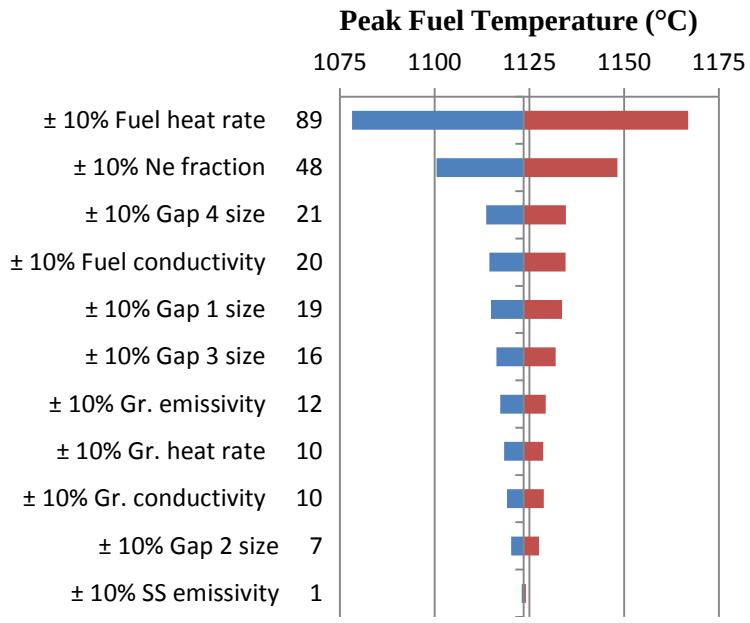

Fig. 2. Sensitivities based on peak fuel temperature in Capsule 5 at EFPD 80.

The input sensitivities combined with uncertainties are used to select the most influential inputs in the thermal models used in the uncertainty quantification for AGR-3/4 capsules. They are fuel heat rate, neon fraction of the gas mixture, four gap sizes, graphite heat rate in the three rings, fuel compact thermal conductivity, and graphite thermal conductivity. The fuel heat rate and neon fraction are selected due to their highest sensitivity coefficients (approximately 0.50 and 0.35 respectively), while their input uncertainties are relatively low (5% for fuel heat rate due to depletion model uncertainty and 3–5% for neon fraction due to flow rate measurement uncertainty [6]). The fuel and graphite thermal conductivities are less sensitive, but they have high input uncertainties (20% and 15% respectively due to lack of direct measurements [6]). The gap size sensitivity coefficients are only in the middle range (about 0.2 for peak fuel temperature). However, complex neutron induced dimensional changes of fuel compacts and graphite rings lead to the gap size modeling assumptions, resulting in increasing gap size uncertainty over time. This uncertainty can contribute significantly to the calculated temperature uncertainty. Even through the graphite heat rate uncertainty is only 3% and its sensitivity coefficient for peak fuel temperature as relatively low, the graphite heat rate is included because of its significant impact on uncertainty of the three graphite rings' temperatures. Finally, the graphite emissivity is not included because of its impact on calculated uncertainty is low.

3. GAP SIZE UNCERTAINTY QUANTIFICATION APPROACH

3.1. Gap Size Uncertainty

As irradiation progresses, the thermal-mechanical properties and structure of the fuel compacts and the three graphite rings are changing due to extended exposure to high temperature and fast neutrons. Typically, under fast neutron irradiation the graphite crystallites expand in the direction of the c-axis and contract in the basal planes [8]. This is because neutron irradiation causes carbon atom displacement [9]. Consequently, the fuel compacts shrink and the graphite rings shrink in most capsules but swell in other few. These dimensional changes result in changes in the gap sizes during irradiation.

As a result, gap sizes are modelled to be axially constant but radially either decreasing or increasing linearly from the start-of-irradiation (SOI) gap size to the end-of-irradiation (EOI) gap size [2,3,4]. The as-fabricated diameter measurements are used to calculate the SOI gap sizes and the PIE diameter

measurements are used for the EOI gap sizes. These gap sizes are adjusted for the graphite material thermal expansion. Taking into account the changes in radius due to fast neutron induced damage and due to material thermal expansion, the graphite radius during irradiation (r_i) is estimated as:

$$r_i = r_0(1 + \frac{\Delta r_n}{r_0} + \frac{\Delta r_{ex}}{r_0}) \quad (1)$$

where r_0 is the as-fabricated radius, Δr_n is the radius change due to fast neutron irradiation, and Δr_{ex} is the radius change due to graphite thermal expansion.

The gap sizes are estimated as the difference between the inner and outer surface radii. For example, the Gap 1 size between the compacts and inner ring can be derived as:

$$G_1 = G_{1\mathrm{SOI}} - \Delta r_{out_{compact}} + \Delta r_{in_{inner\ ring}} \quad (2)$$

where G_{1SOI} is the SOI Gap 1 size estimated from as-fabricated measurements, $\Delta r_{out_{compact}}$ is the capsule averaged radius change in fuel compacts, and $\Delta r_{in_{inner\ ring}}$ is the inner radius change in the inner ring. The uncertainty of gap size expressed in Eq. (2) is quantified using standard uncertainty propagation formula as:

$$\sigma_{G_1} = \sqrt{\sigma^2_{G_{1SOI}} + \sigma^2_{\Delta r_{out_{compact}}} + \sigma^2_{\Delta r_{in_{inner\ ring}}}} \quad (3)$$

where $\sigma_{G_{1SOI}}$ is the uncertainty of the SOI Gap 1 size; $\sigma_{\Delta r_{out_{compact}}}$ and $\sigma_{\Delta r_{in_{inner\ ring}}}$ are the uncertainties of radius changes in compacts and shell inner ring, respectively. The radius change uncertainties come from three main sources: (i) measurement uncertainty (e.g., fabrication and PIE diameter measurements), (ii) uncertainty of material properties (i.e., thermal expansion coefficient), and (iii) modeling assumptions (e.g., difference between modeled and PIE gap sizes).

3.1.1. Measurement uncertainty

Fabrication measurement uncertainty – During the assembly, diameters of all components were measured and reported with measurement uncertainties. These measurement uncertainties result in 0.0254 mm as-fabricated gap size uncertainty for the four gaps in all capsules.

PIE measurement uncertainty – During the PIE, diameters of the fuel compacts, three graphite rings, and the stainless steel shells are measured with high precision procedures. The diameter change ratios (calculated as the difference between PIE and as-fabricated diameters divided by the as-fabricated diameter) and associated uncertainties are reported in [10].

However, necessary diameters cannot be measured in several fuel body capsules. The fuel compacts and inner rings in these capsules are not accessible to measure due to essential safety testing, which requires keeping the fuel body (the fuel compacts, inner ring, and outer ring) together. These missing PIE diameter change ratios have been estimated based on available diameter change ratios from other capsules. This is because diameter change ratios are consistent across capsules and exhibit strong dependency on fast fluence. A regression function [$f(f)$] which closely approximates the set of diameter change ratios measured at PIE for each diameter (i.e., inner diameter of inner ring) is established as follows [11]:

$$\Delta r/r_0 \approx f(f) + N(0, \sigma^2) \quad (4)$$

This regression function can be used to predict the missing PIE diameter change ratios at calculated fluence. The SAS linear regression routine *proc reg* was used for fitting the data [12]. Together with parameter estimates, this routine also provides prediction intervals for change ratios (not yet observed) corresponding to levels of fast fluence. With probability 1-α, the predicted radius change ratio will stay within the following prediction intervals:

$$\Delta r/r_0 \ \in f(f) \pm t_{\nu,\alpha/2}\hat{\sigma}\left(1+\frac{1}{n}+\frac{(f-\bar{f})^2}{(n-1)s^2}\right)^{1/2}$$

where ν represents the degrees of freedom, α is the desired significance level, n is the number of data points, s is variance, and $\hat{\sigma}$ is standard deviation estimated from provided data. When 1-α=95% and degree of freedom (ν) is high (adequate data points (n) for fitting), the prediction intervals equal at least two standard deviations; therefore the standard deviation of the predicted radius change ratio can be estimated as:

$$\sigma_{\Delta r/r_0\ pred} = (U95 - L95)/4 \quad (5)$$

where $U95, L95$ are the upper and lower 95% prediction intervals for individual predicted radius change ratio. That is, the EOI radius change ratio uncertainty can be estimated from provided PIE radius change ratio uncertainties when they are available. In case of missing PIE dimension measurement; the uncertainty of predicted radius change ratio in Eq. 5 is used.

3.1.2. Thermal expansion uncertainty

It is well-known that materials expand when they are exposed to high temperature, which is characterized by the expansion coefficient. The graphite thermal expansion coefficients are measured for nuclear grade graphite specimens irradiated in the advanced graphite creep (AGC) experiment at various temperatures and doses of fast neutron fluence. A model was fit to the observed data, resulting in the following function for thermal expansion coefficients in (m/m ˚C):

$$\alpha_L = 4x10^{-6}(1 + af^2 + bf + cf^2 * T + df * T) \quad (6)$$

where α_L is the linear thermal expansion coefficient in (m/m ˚C); a, b, c, and d are the coefficients estimated by best fitting to measured diameter change ratios of the AGC graphite specimens ($a=4.25x10^{-3}$; $b=2.09x10^{-2}$; $c=-5.63x10^{-6}$; and $d=7.96x10^{-6}$); T is graphite temperature in Fahrenheit; and f is fast fluence in 10^{25} n/m^2 [E>0.18MeV]. The diameter change ratio due to thermal expansion at high temperature (T) relative to room temperature (T_0) is estimated as:

$$\Delta r_{ex}/r_0 = \alpha_L(T - T_0) \quad (7)$$

Since the thermal expansion coefficients for fuel compacts and the three graphite ring are similar, the thermal expansion impacts only Gap 4 between the sink ring and stainless steel shell and has negligible impact on the remaining three gaps. For the AGR-3/4 temperature range, the sink ring outer radius would increase by approximately 0.05 mm on average and the stainless steel shell inner radius would increase by approximately by 0.02 mm (given stainless steel thermal expansion coefficient of $1.73x10^{-5}$ m/m-˚C and temperature of ~100 ˚C). As a result, the Gap 4 size would decrease by approximately 0.03 mm. Because of the lack of direct thermal expansion coefficient data for graphite materials used in AGR-3/4 capsule, it is reasonable to assume that the thermal expansion coefficient uncertainty is 20%. Therefore, the gap size uncertainty due to the thermal expansion coefficient uncertainty can be estimate as 20% of the change in Gap 4 (20% of 0.03mm), which equals 0.006 mm.

3.1.3. Gap size modeling bias

A gap size modeling bias is the difference between gap size used in the thermal model and actual gap size (either measured or predicted). Therefore, gap size modeling bias can be expressed as:

$$B_{G_{EOI}} = G_{PIE} - G_{EOI} \quad (8)$$

3.2. Gap Size Uncertainty Quantification

Since the as-fabricated diameter measurements are used to calculate the SOI gap sizes and the PIE diameter measurements are used for estimating the EOI gap sizes, it is reasonable to assume zero gap size modeling bias for all AGR-3/4 capsules.

Start-of-irradiation gap size uncertainty - Since the SOI gap sizes are estimated from the as-fabricated diameter measurements, the uncertainty of the SOI gap size is estimated based on the tolerance error of as-fabricated diameters of 0.0254 mm. Including the gap size uncertainty due to thermal expansion, the SOI gap size uncertainty for all AGR capsules can be estimated as:

$$\sigma_{G_{SOI}} = \sqrt{0.0254^2 + \sigma_{G_{TE}}^2} \tag{9}$$

End-of-irradiation gap size uncertainty - The uncertainty of EOI gap size is estimated by combining three uncertainty sources: the PIE gap size measurement uncertainty ($\sigma_{G_{PIE}}$) and gap size uncertainty due to material thermal expansion ($\sigma_{G_{TE}}$). Thus, the EOI gap size uncertainty can be expressed as:

$$\sigma_{G_{EOI}} = \sqrt{\sigma_{G_{PIE}}^2 + \sigma_{G_{TE}}^2} \tag{10}$$

Daily gap size uncertainty - The neutron induced dimensional changes of fuel compacts and graphite components increase proportionally with fast fluence. Therefore, it is reasonable to assume that the gap size uncertainties in terms of absolute values are also increasing over time. Assuming the gap size uncertainty is increasing from the SOI to the EOI gap size uncertainty, the daily gap size uncertainty estimated as linear function of fast fluence as:

$$\sigma_{G_i} = \frac{\left(\sigma_{G_{EOI}} - \sigma_{G_{SOI}}\right) * f_i}{f_{EOI}} \tag{11}$$

where f_i and f_{EOI} are the accumulative fast fluence on day (i) and at end of irradiation, respectively.

4. AGR-3/4 GAP SIZE UNCERTAINTY AND TEMPERATURE UNCERTAINTY

4.1. PIE Diameter Measurements

Diameter change data of the fuel compacts, the three graphite rings, and the shell were extracted from the AGR-3/4 PIE metrology data report [10]. The reported results are radius change ratios ($\Delta r / r_0$) and associated uncertainties. Among twelve capsules, there are five fuel body capsules, where fuel compacts, inner ring, and outer ring are kept together for the required safety testing. Therefore, no dimensional data for compacts, inner ring, and inner diameter of outer ring were measured for these fuel body capsules. Fig. 3 presents the radius change ratios as a function of fast fluence for fuel compacts from the three AGR experiments (on the left side) and for the AGR-3/4 three graphite rings (on the right side).

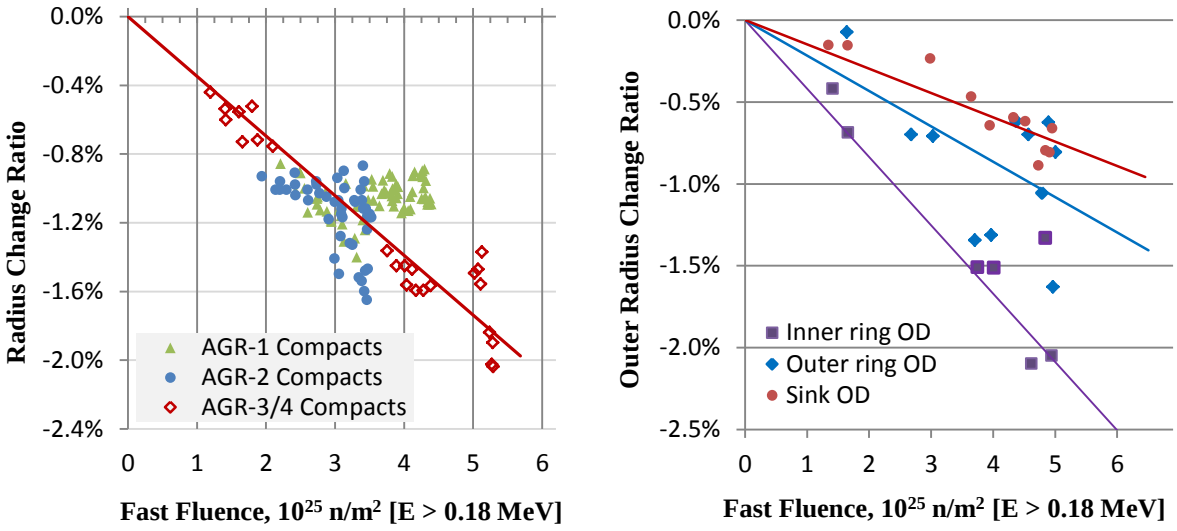

Fig. 3. AGR compact radius change ratios (left) and AGR-3/4 radius change ratios of the AGR-3/4 three graphite rings (right) as function of fast fluence.

AGR-3/4 compact radius change ratios (empty diamonds) are fit fairly well with a linear function of fast fluence (red line). The AGR-1 (triangles) and AGR-2 (dots) compact radius change ratios line up nicely with the AGR-3/4 compact data. This indicates a strong linear relationship between compact radius change ratios and fast fluence. The plots of outer diameter (OD) change ratios of the three graphite rings also exhibit the consistency and dependency of fast neutron induced shrinkage of graphite materials. Even though, materials used in the three rings are from different nuclear graphite grades (i.e., matrix blank, IG-110, and PCEA) the OD change ratios of the three graphite rings display the downward trend as function of fast fluence. The effect of temperature on shrinkage rate is apparent here. The lowest temperature range of the sink rings (500 – 700˚C) leads to a lower shrinkage rate, as indicated by the smaller slope of the fitted line (red line). The higher temperature range (800 – 1100˚C) of the inner ring results in higher shrinkage rate, as indicated by the steeper slope of the fitted line (purple line).

4.2. Gap Sizes and Uncertainty

The consistency of graphite shrinkage rate in different capsules allows the use of best-fit functions to predict the radius change ratio for capsules where the required PIE data are not measured. The OD and inner diameter (ID) change ratios and fitted lines for the fuel compacts and three graphite rings as a function of fast fluence are presented on the left side of Fig. 4. At start of irradiation, when fast fluence equals zero, all diameters are unchanged. Thus, no-intercept polynomials are used to fit the PIE diameter change ratios. All fitted functions are statistically significant, as indicated by the narrow confident intervals of the mean (dark green bands). The 95% confidence intervals for individual predictions (light shaded bands) for each diameter show the acceptable prediction uncertainty. The PIE predicted and measured uncertainties of the OD and ID change ratios in terms of percent (%) of as-fabricated radius are presented in the table on the right side of Fig. 4. For ODs (green color in plots on the left side of Fig. 4), change ratios of fuel compacts and three rings are fit well with a linear function of fast fluence, as indicated by the narrow confidence intervals of the mean. For IDs (orange color in plots on the left side of Fig. 4), the change ratios for the inner ring and outer ring are positive and for the sink ring are negative (bottom panel). The second order polynomials yield a better fit to the ID change ratios.

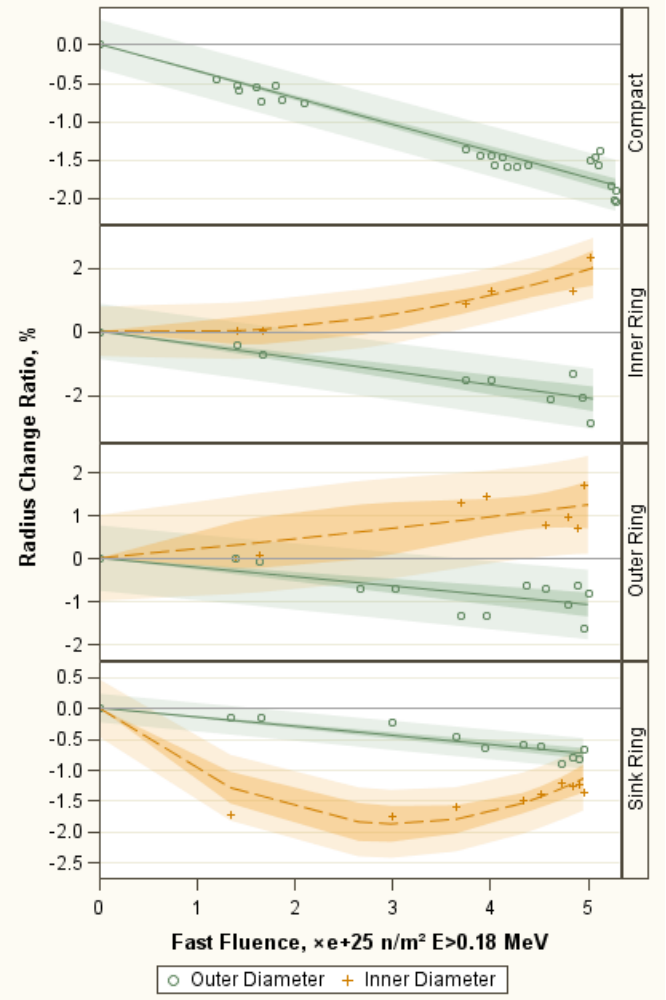

Measured and predicted uncertainties of the PIE radius change ratios

Diameter	$\sigma_{\Delta r/r_{0\,Pred}}$, % of r_0	$\sigma_{\Delta r/r_{0\,PIE}}$, % of r_0
Compacts OD	0.163	0.067
Inner ring ID	0.444	0.275
Inner ring OD	0.455	0.113
Outer ring ID	0.480	0.077
Outer ring OD	0.394	0.085
Sink ring ID	0.257	0.029
Sink ring OD	0.120	0.038

Fig. 4. Left side: PIE diameter change ratios and fitted lines for ODs and IDs of compacts and graphite rings with 95% confidence intervals of the mean (dark color) and prediction (light color) and right side: Measured and predicted uncertainties of the PIE radius change ratios.

The SOI and EOI gap sizes with uncertainties in terms of one standard deviation are presented in Fig. 5 for the twelve AGR-3/4 capsules. The largest gap changes are seen in the middle capsules due to larger radius changes at higher fast fluence. Three gap sizes (1, 2, and 4) increase with time in all twelve capsules. Gap 3 decreases in nine capsules and increases in three capsules (1, 3, and 11). Gap 3 in Capsules 4, 5, 6, and 9 is almost closed (~0.15 mm) at the end of irradiation.

The SOI gap size uncertainty equals 0.0261 mm for four gaps in all capsules, which include uncertainty of 0.0254 mm due to gap size as-fabricated uncertainty and of 0.006 mm due to 20% uncertainty of thermal expansion coefficient (Equation 9). The EOI gap size uncertainties are estimated using Equation 10 as described above. For EOI gap size calculated from the PIE measured diameters, the measurement uncertainties of radius change ratios (last column in table on the right side of Fig. 4) are used for gap size uncertainty quantification, otherwise the higher prediction uncertainties of radius change ratio (middle column in table on the right) are used. Thus, the EOI gap size uncertainties are higher for Gap 1 and Gap 2 in the four fuel body capsules (2, 6, 9, and 11), where the compact and inner ring diameters are not measured.

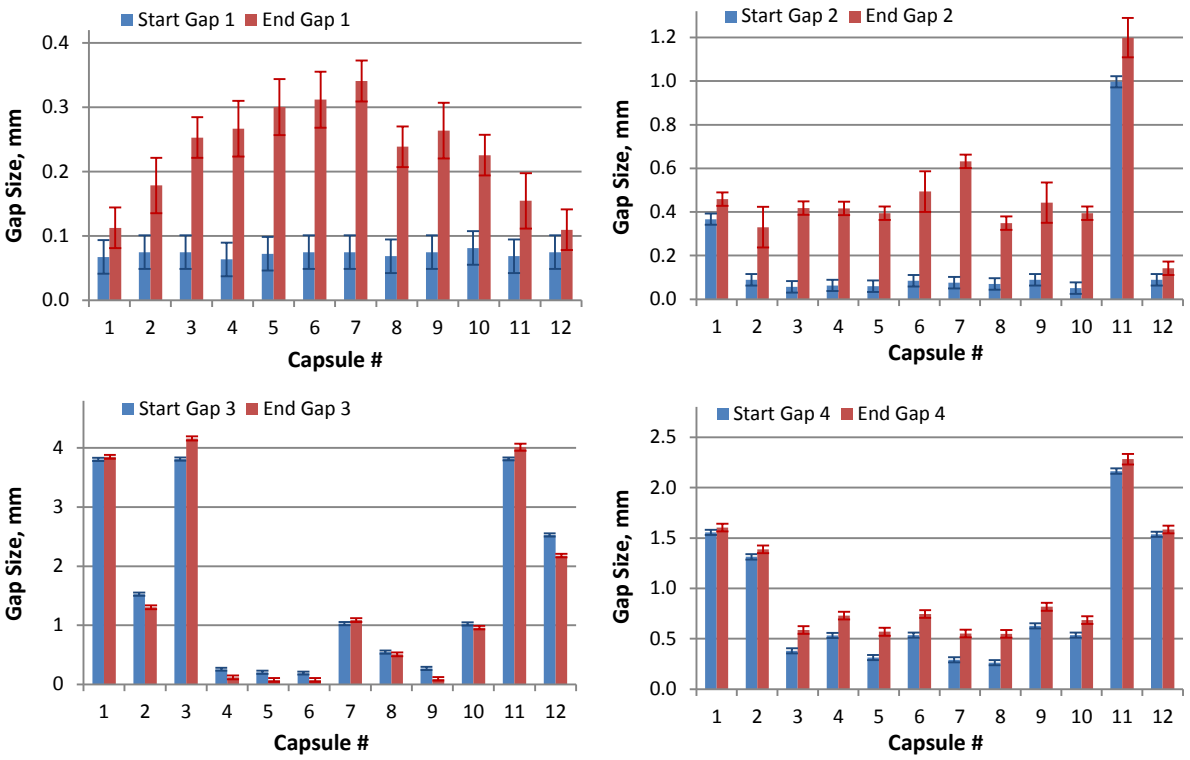

Fig. 5. SOI and EOI gap sizes and uncertainties for four gaps in AGR-3/4 capsules.

4.3. Calculated Temperature Uncertainty

As the gap sizes are varying linearly with irradiation time, the daily gap size absolute uncertainties are also anticipated to vary linearly with time from the SOI to the EOI values. The gap size relative uncertainties for twelve capsules are presented on the left side of Fig. 6. These uncertainties are not linear over time due to changes in both gap sizes and associated uncertainties. The relative gap size uncertainties decrease over time for Gaps 1 and 2 because the increase in absolute gap size uncertainty is smaller than increase in gap sizes. The increases in relative uncertainties of Gap 3 in Capsules 4, 5, 6, and 9 near the end of irradiation are due to small EOI gap sizes in these capsules.

The impact of gap size uncertainties on calculated fuel temperature can be seen in the plot on the right of Fig. 6, which depicts the daily uncertainty results as a function of EFPD for peak fuel temperature in Capsule 9. The daily relative uncertainties of the nine influential inputs are presented in the first panel. Uncertainties of fuel heat rate (5%), graphite heat rate (3%), fuel thermal conductivity (20%), and graphite thermal conductivity (15%) are constant over the entire irradiation and are the same for all capsules. On the other hand, the uncertainties of four gap sizes are dynamic over the irradiation time as described in previous section. The variable neon fraction uncertainty due to the flow meter measurement uncertainty is estimated as a function of neon fraction [6]. Panel 2 shows the nine input sensitivity coefficients for peak fuel temperature. The heat rate sensitivity is highest following by neon fraction, graphite heat rate, and Gap 4. Sensitivities of the remaining three gaps are small (less than 0.1). Finally, sensitivities of fuel compact thermal conductivity (purple line) and of graphite thermal conductivity (orange line) are small and negative (around -0.1).

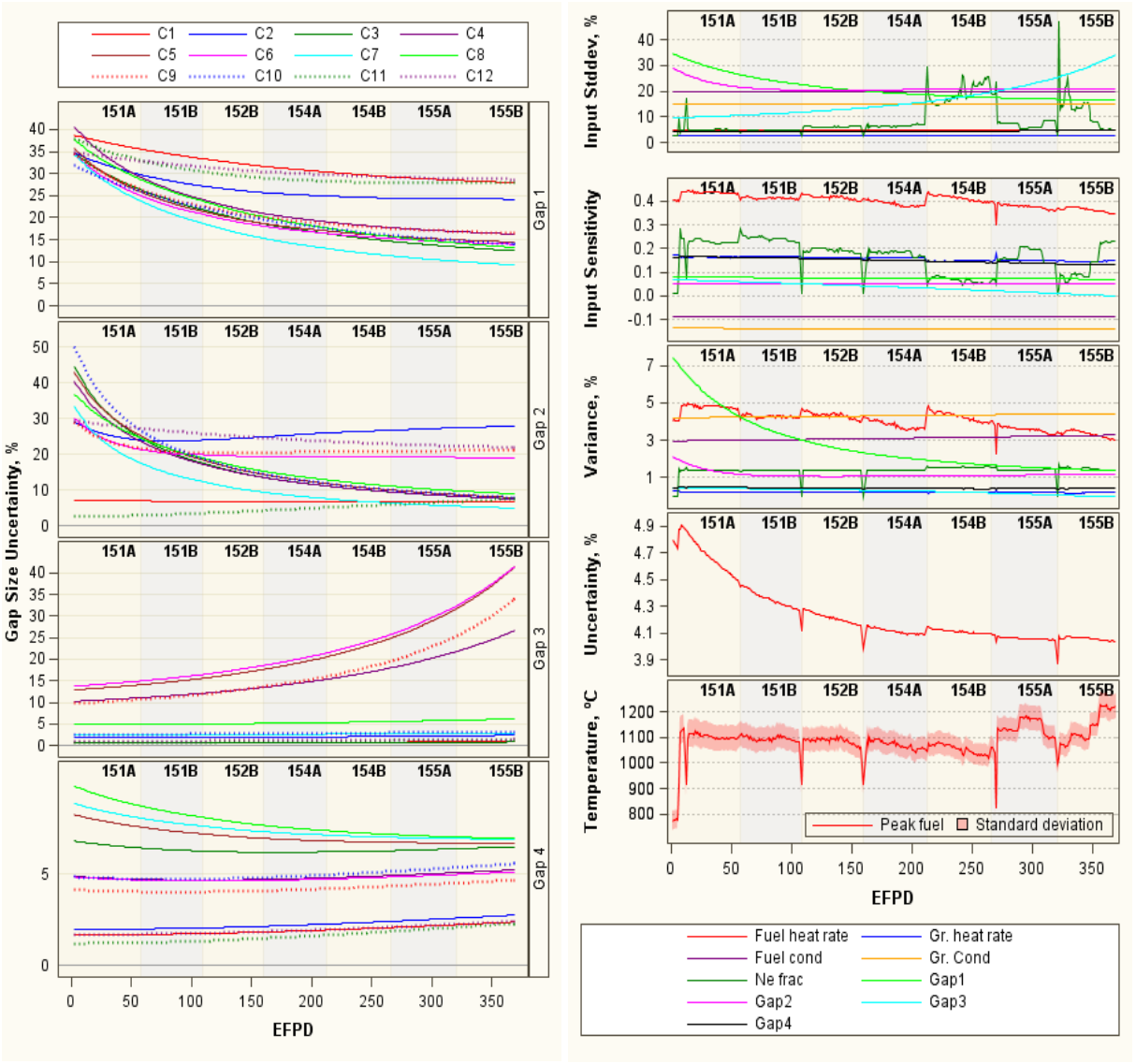

Fig. 6. Daily gap size relative uncertainties for twelve capsules (left) and Capsule 9 daily uncertainty analysis results for peak fuel temperature (right).

The weighted variances of peak fuel temperature in Panel 3 show that the fuel heat rate and graphite conductivity are the dominant factors for uncertainty of peak fuel temperatures during most irradiation cycles. However, the high uncertainty of Gap 1 is the dominant factor for peak fuel temperature during the first cycle (151A) and then its impact decreases with decreasing relative uncertainty due to increase in gap size. The peak fuel temperature relative uncertainty in terms of one standard deviation presented in Panel 4 is decreasing with time because of the decreasing Gap 1 and Gap 2 uncertainties over time as shown in Panel 1. The last panel shows calculated daily peak fuel temperatures with associated uncertainties as a function of EFPD. The peak fuel temperature uncertainties in Capsule 9 are decreasing from 55 ˚C at the start of irradiation to 33 ˚C at the end of irradiation. It is worth mentioning that the PIE metrology data used for estimating the EOI gap sizes helped reduce gap size uncertainties leading to reduction of AGR-3/4 temperature uncertainty.

Table 2 presents uncertainties of calculated volume-average (VA) and peak fuel temperatures (FT) and peripheral TC1/2 temperatures for the twelve capsules. Since uncertainties of the nine selected inputs are similar in all capsules, the difference in calculated temperature uncertainty across capsules is determined mainly by the model biases as shown in Table 1. Capsules 2, 7, and 10 have the lowest

temperature uncertainty because of their negligible model bias and low uncertainties of the four gap sizes. Capsules 3 and 9 have slightly higher temperature uncertainty due to higher model bias and gap size uncertainties. Capsule 11 has the highest temperature uncertainty (up to 138˚C or more than 10%) due to high model bias (9.9% as shown in Table 1). The peak fuel temperature uncertainty is 4–5% for the six remaining capsules.

Table 2. Calculated temperature uncertainties in ˚C

	Capsule	12	11	10	9	8	7	6	5	4	3	2	1
VA FT	Maximum	49	132	39	48	58	45	53	55	50	44	35	43
	Average	46	125	30	39	45	33	45	40	41	36	32	40
Peak FT	Maximum	52	138	45	55	66	53	62	65	58	50	41	47
	Average	49	131	34	46	50	38	52	48	48	40	37	44
TC1/2	Maximum	29	83	20	21	32	26	26	22	23	23	17	25
	Average	27	76	18	17	26	22	21	20	19	21	16	22

5. CONCLUSION

Under irradiation, diameters of fuel compacts reduce proportionally with fast fluence and these changes are fairly consistent across all AGR capsules. The radius change ratios reached 2% at fast fluence of 5.27 (10^{25} n/m^2, E>0.18MeV), which occurred in AGR-3/4 Capsule 7. The inner and outer diameter changes are consistent for the three graphite rings, except for the sink ring inner diameter. In general, the diameter changes of fuel compacts and graphite components are less than 2% for all capsules. These dimensional measurements of fuel compacts and three graphite rings obtained during PIE are used for establishing the gap size variation models used in the thermal simulation codes.

Complex behavior of fuel compacts and graphite components under irradiation could lead to high uncertainty of gap sizes in AGR-3/4 capsules. However, the large number of PIE diameter measurements and the large variation in fast fluence in the twelve capsules allows establishing functional relationship between diameter change ratios and fast fluence that can be used to estimate gap sizes. The narrow confidence limits for the fitted functions lead to relatively small uncertainty of the predicted radius change ratios, which keep the gap size uncertainties low for capsules where the PIE dimensional data are not available.

Among the four gas gap sizes, Gap 1 and Gap 2 (about 0.075 mm widths) have the highest relative input uncertainty (up to 30% at the start of irradiation). Even though gap sensitivities are generally small (less than 0.1), the highest Gap 1 uncertainty is the second most significant factor contributing to uncertainty of the fuel temperature predictions. On the other hand, Gap 3 and Gap 4 have much lower relative uncertainties due to larger gap sizes, which lead to smaller impact on uncertainty of fuel and graphite temperatures. The high Gap 4 sensitivity to calculated TC temperatures led to high impact on temperature uncertainties of TC1 and TC2, which are located near this gas gap. In general, the PIE diameter measurements help reducing the uncertainty of gap sizes, which leads to reduction of calculated temperature uncertainties.

ACKNOWLEDGMENT

The authors would like to thank James Sterbentz and Joe Palmer of Idaho National Laboratory for their comments and supports. This work was supported and funded by the U.S. Department of Energy, INL ART TDO Program, Idaho Operations Office Contract DE-AC07-05ID14517.

REFERENCES

1. INL, "Technical Program Plan for INL Advanced Reactor Technologies Technology Development Office/Advanced Gas Reactor Fuel Development and Qualification Program," PLN-3636, Rev. 4, Idaho National Laboratory, (2015).
2. G. L. Hawkes, J. W. Sterbentz, and J. T. Maki, "Daily Thermal Predictions of the AGR-3/4 Experiment With Time-Varying Gas Gaps," *Nucl. Eng. and Rad. Sci*., **1/041012**(1), (2015).
3. G. L. Hawkes, J. W. Sterbentz, J. T. Maki, and B. T. Pham, "Daily Thermal Predictions of the AGR-1 Experiment With Gas Gaps Varying With Time," ICAPP 2012 Conference, Chicago, IL, Jun. 2012, Paper No. 12111, (2012).
4. G. L. Hawkes, J. W. Sterbentz, and B. T. Pham, "Thermal Predictions of the AGR-2 Experiment With Variable Gas Gaps," *Nucl. Technol*., **190**(3), 10.1382/NT14-73, (2015).
5. B. T. Pham, G. L. Hawkes, and J. J. Einerson, "Improving Thermal Model Prediction through Statistical Analysis of Irradiation and Post Irradiation Data from AGR Experiments," *Nucl. Eng. and Design*, Vol. **271**, pp. 209-216, (2014).
6. B. T. Pham, G. L. Hawkes, and J. J. Einerson, "Uncertainty Quantification of Calculated Temperatures for Advanced Gas Reactor Fuel Irradiation Experiments," Proceeding of NURETH-16, paper # 14086, Chicago, IL, August 29 – September 2, (2015).
7. G. L. Hawkes, J. W. Sterbentz, and B. T. Pham, "Sensitivity Evaluation of the AGR- 3/4 Experiment Thermal Model Irradiated in the Advanced Test Reactor," Proceedings of the ASME IMECE2015, Paper No. 53544, International Mechanical Engineering Congress & Exposition Conference, Houston, Texas, November 13-19, (2015).
8. P.R. Goggin, et.al., "Dimensional changes in the Irradiated Graphite Lattice," *Carbon 1964*, Vol. **1**, pp. 189-200, Pergamon Press Ltd., Printed in Great Britain, (1964).
9. J.H.W. Simmons, *Radiation Damage in Graphite*, First edition, Pergamon Press Ltd., (1965).
10. J.D. Stempien, F.J. Rice, P.L. Winston, and J.M. Harp, "AGR-3/4 Irradaiation Test Train Disassembly and Component Metrology First Look Report," INL/EXT-16-38005, (2016).
11. N. Draper, and H. Smith, *Applied Linear Regression*, 2nd edition. John Wiley: New York, (1981).
12. SAS Institute Inc., *SAS/STAT® 12.3 User's Guide*. Cary, NC: SAS Institute Inc., (2013)